



NetworkGT: A GIS tool for geometric and topological analysis of two-dimensional fracture networks

Björn Nyberg¹, Casey W. Nixon¹, and David J. Sanderson²

¹Department of Earth Sciences, University of Bergen, P.O. Box 7803, 5020 Bergen, Norway

²Faculty of Engineering and the Environment, University of Southampton, Southampton SO17 1BJ, UK

ABSTRACT

Fractures rarely occur individually but more usually as networks of numerous fractures whose arrangement, abundance, and interaction control the mechanical and transport properties of rock masses. Of particular importance are the distributions and spatial variations of different geometric (locations, orientation, length, etc.) and topological (intersections, connectivity, etc.) attributes of fractures in a network. Geographical Information Systems (GIS) provide a means to map and digitize two-dimensional fracture networks from a variety of field and remote sensing data and to display the results in the form of quality maps. We introduce NetworkGT, an open-source toolbox for ArcGIS capable of efficient sampling, analysis, and spatial mapping of geometric and topological attributes of two-dimensional fracture networks. The toolbox helps to extract and plot geometric and topological information from a given two-dimensional fracture network including: rose diagrams, plots of frequency distribution and topology, and maps of topological parameters. Using a fracture network example from offshore NW Devon, United Kingdom, we illustrate the practicality and effectiveness of the toolbox. This includes computing a contour grid with 1326 subsampled regions within the fracture network, which is used to demonstrate the quantitative capabilities of the toolbox and the ability to spatially map important network properties. The toolbox will help to facilitate the increasing application of geometry and topology in the analysis and comparison of fracture networks at a range of scales. Furthermore, the integration of the NetworkGT toolbox into ArcGIS allows two-dimensional fracture networks to be interpreted, mapped, and fully analyzed within the same software package.

INTRODUCTION

A fracture network could comprise numerous fractures that show a range of orientations and lengths with the potential to form an interconnected network (Peacock et al., 2016). Fractures sharing similar characteristics often form distinct fracture sets, which may or may not intersect, and that evolve to vary in their spatial distribution (Berkowitz, 2002). The abundance and arrangement

of fractures relate directly to parameters describing rock mechanical (stiffness and strength) and transport properties such as porosity and permeability (e.g., Adler and Thovert, 1999; Zimmerman and Main, 2003; Adler et al., 2013). Thus, measuring, characterizing, and assessing the connectivity of fracture networks are important tasks in many areas of geosciences and geoenvironment, including the exploration and production of hydrocarbons, geothermal energy, and water resources.

Fracture networks can be analyzed in terms of their geometry and topology (Peacock et al., 2016). Individual fractures within a two-dimensional network are measured for geometries such as orientation, length, spacing, and intensity, with a view to determining fracture density, size frequency distributions (Johnston and McCaffrey, 1996; Bonnet et al., 2001) and characterizing their spatial distributions (Gillespie et al., 1993; Putz-Perrier and Sanderson, 2008; Nixon et al., 2014). More recently, topological analysis of fracture networks has been established, focusing on characterizing the arrangement and connectivity of fractures within a network (Manzocchi, 2002; Sanderson and Nixon, 2015). Network topology describes the geometric relationships between fractures using components, such as nodes and branches, and dimensionless parameters that are invariant to scale, strain, and continuous transformation within the network (Huseby et al., 1997; Jing and Stephansson, 1997; Sanderson and Nixon, 2015). Topology is essential for the characterization of fracture networks and quantifies fracture connectivity directly, providing parameters for evaluating the percolation potential of a network (Manzocchi, 2002). Field mapping provides a means to map fractures but is often time consuming and spatially limited to the outcrops. Digitization of fracture networks from imagery (unmanned aerial vehicle [UAV], aerial photography, satellite imagery, light detection and ranging [LiDAR], etc.) within Geographical Information Systems (GIS) is more efficient and essential for a robust analysis and characterization (McCaffrey et al., 2005; Nixon et al., 2011; Bemis et al., 2014; Bisdom et al., 2017).

A number of software packages and programs have been developed for basic fracture analysis, mainly focusing on analysis of fracture length and orientation (e.g., FracMan7, 2012) or spatial sampling and analyses of fracture networks (e.g., FraNEP by Zeeb et al., 2013). These are often developed for specific purposes or individual studies and thus have limited applications.

Furthermore, they are mainly focused on extracting geometric statistics of fracture patterns, producing rose diagrams, and length-frequency distribution plots, etc., but these software packages do not implement a topological analysis of fracture networks. FracPaQ and ADFNE are both matrix laboratory (MATLAB)-based packages by Healy et al. (2016) and Fadakar-A (2017), respectively; these packages take a substantial step forward in fracture network analysis incorporating both geometric and topological analysis. However, FracPaQ and ADFNE both require manual fracture interpretations to be imported from other digitization software; data sets are not spatially georeferenced and require a certain level of coding experience. They do not implement the visualization or statistical analysis of fracture network block sizes, and FracPac does not include cluster analysis. Thus, NetworkGT was designed to incorporate topological analysis through the representation of the network by a series of branches and nodes, and the analysis of resulting parameters such as connections per branch provides essential information on fracture network connectivity (Sanderson and Nixon, 2015). Node and branch counting provides a simple and efficient method for analysis of natural fracture networks (e.g., Richards et al., 2015; Morley and Nixon, 2016; Dimmen et al., 2017; Procter and Sanderson, 2018), and NetworkGT provides a suite of algorithms to do this within the mapping environment of ArcGIS.

GIS provides a means to spatially map, visualize, and analyze fracture networks from georeferenced imagery (e.g., Alberti, 2005; Bhattacharyya and Czeck, 2008; Nixon et al., 2011; Hardebol and Bertotti, 2013; Kociánová and Melichar, 2016). It preserves the spatial positions of fractures and intersections rather than just analyzing lengths and orientations, providing two significant advantages in the analysis of fractures:

- (1) By linking each geometric attribute to its spatial position, it is possible to analyze these attributes across a range of different spatially arranged subsets that can be controlled by the user. Data may also be grouped to other spatial information, such as mapped lithology and proximity to structural features.
- (2) The relative position and type of linkage between any two fracture traces allow for topological analysis, e.g., comparison of type and frequency of connecting nodes. Thus the topology and geometry may be used to spatially compare natural fracture networks on a regional or continental scale.

GIS tools such as DigiFract (Hardebol and Bertotti, 2013) collect fracture spatial data to analyze their orientation and length-frequency distributions from scan line and scan windows. Though the software incorporates an improved fracture digitization framework, topological classification is not implemented, and geometric measurements are also limited. To our knowledge, no existing, comprehensive GIS toolkit exists for the specific purpose of objectively and automatically extracting both the geometric and topological information from digitized fracture networks.

The aim of this paper is to present NetworkGT (Network Geometry and Topology), an open-source ArcGIS toolbox developed specifically for the quantitative geometric and topological analysis of fracture networks. NetworkGT fo-

cuses on the analysis of two-dimensional networks because three-dimensional rock volumes are difficult to sample completely, and most available data or samples are two-dimensional (e.g., fracture trace maps, well-bore image logs, rock slab surfaces, etc.). The ArcGIS framework provides a graphical interface to develop and integrate workflows using the large suite of existing GIS tools. NetworkGT is designed to efficiently sample, analyze, and spatially map geometric and topological attributes of large two-dimensional fracture networks.

■ NetworkGT TOOLBOX

The NetworkGT toolbox consists of 18 tools within the ArcGIS (version 10.4; ESRI, 2016) to focus on three main aspects of two-dimensional fracture network analysis: sampling, geometry, and topology. The algorithms rely on a set of Python-based programming scripts to geometrically and topologically analyze and plot statistical information of two-dimensional fracture networks. The algorithm behind each tool and a suggested workflow are discussed and demonstrated in detail below using conceptual diagrams and the data set of Nixon et al. (2012), who interpreted 486 seafloor fracture traces based on high-resolution, multibeam bathymetry offshore NW Devon, UK. The toolbox, data set, installation procedure, and a user guide demonstrating a detailed workflow are provided in the Supplemental Information¹ of this article. A simple flow chart illustrates the workflow of the NetworkGT toolkit (Fig. 1).

As a basic input, the toolkit requires a geospatially and topologically consistent digitized fracture network (e.g., Fig. 2), with a projected coordinate system that is either imported or interpreted within a GIS environment. Digitization of two-dimensional fracture networks from remotely sensed information is appropriate in areas of undulating topography where relief varies by less than 10%–20% of the maximum fracture length (Healy et al., 2016). If three-dimensional data are available (e.g., LiDAR and photogrammetry), a two-dimensional digitization surface can be used on the topography of the fracture network to correct for length distortions (Hardebol and Bertotti, 2013). In addition to the digitized fracture network, an optional boundary (Fig. 3A) may be used to clip the extent at which fractures in the network will be interpreted. This may address uncertainties in fracture network delineations by excluding geometric and topological analyses where data quality is poor (for example, vegetation, scree, and/or resolution issues on outcrops).

It is important that individual fractures are interpreted as a single digitized line, to preserve fracture-length characteristics, and that fractures intersect at the same digitized point (or node), which may be easily facilitated by using the snapping option when digitizing. Topologically inconsistent digitization of fracture networks may be repaired by the “repair network” tool, which resolves common topological errors (Fig. 2) associated with either manual or automated fracture network digitization workflows.

An array of analytical tools is available to allow the extraction of geometric and topological data from the network. The tools create a number of output formats and visualization options (including graphs, tables, and maps). One

| NetworkGT Toolbox | |
|--|---|
| Version 0.1 | |
| Björn Nyberg ^{1*} , Casey W. Nixon ¹ , David J. Sanderson ² | |
| Department of Earth Sciences, University of Bergen, P.O. Box 7803, 5020 Bergen, Norway; ¹ | |
| Faculty of Engineering and the Environment, University of Southampton, Southampton SO17 1BJ, UK ² | |
| *Corresponding Author: bjorn.nyberg@iuh.no | |
| Contents | |
| 1.0 | Background..... 2 |
| 1.1 | Citation and Acknowledgments 2 |
| 1.2 | License 2 |
| 2.0 | Installation..... 3 |
| 2.1 | NetworkGT Download 3 |
| 2.2 | Python Installation 3 |
| 2.3 | NetworkGT Toolbox Installation..... 3 |
| 3.0 | Workflow..... 4 |
| 3.1 | Digitizing Fracture Network..... 4 |
| 3.2 | Geometrical Analysis..... 5 |
| 3.3 | Topological Analysis..... 7 |
| 3.4 | Spatial Analyses..... 11 |
| 4.0 | Contact Information & Feedback 14 |

¹Supplemental Information. Toolbox, data set, installation procedure, and a user guide demonstrating a detailed workflow are provided. Please visit <https://doi.org/10.1130/GES01595.S1> or the full-text article on www.gsapubs.org to view the Supplemental Information. For future upgrades and community involvement with the software contribution, the authors have also made these resources available at GitHub, <http://github.com/BjornNyberg/NetworkGT/releases>.

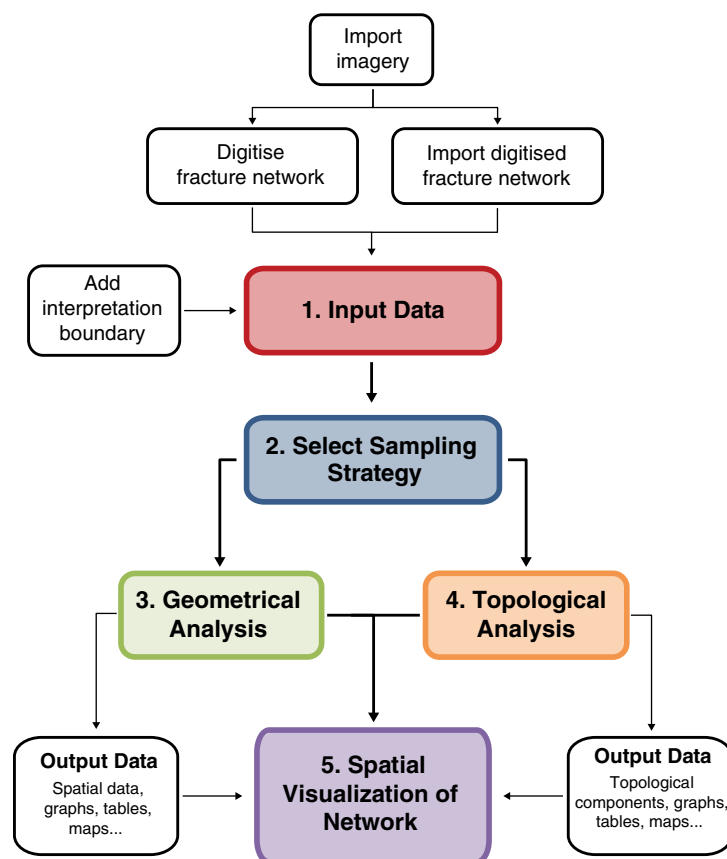


Figure 1. Flowchart showing the NetworkGT workflow: (1) input data; (2) select sampling strategy; (3) geometrical analysis; (4) topological analysis; and (5) spatial visualization of geometric and topological parameters.

particularly novel aspect of the toolkit is the ability to subsample the network and, hence, investigate spatial variations and identify any areas of interest within the network.

SAMPLING STRATEGIES

A number of strategies exist for sampling the fracture network depending on its scale and spatial extent and the purpose of the analysis (Watkins et al., 2015). In field studies, it can be difficult to collect data for the whole network; hence, linear scanlines (Priest, 1993) and circular scanlines (Mauldon et al.,

2001; Rohrbaugh et al., 2002; Procter and Sanderson, 2018) are often preferred sampling strategies for collecting data efficiently. Areal sampling, on the other hand, involves collecting fracture data in two dimensions in the form of fracture maps (Nixon et al., 2011), providing a means to assess the network as a whole as well as investigating spatial variability. For diversity, the NetworkGT toolbox provides a number of sampling options (summarized below) that allow the end user to customize their assessment of the fracture network.

Polygon Sampling

Polygon sampling allows two-dimensional areal sampling of a digitized fracture network for analysis. A manual area sampling (Fig. 3A) is used to define one or multiple user-defined subsampled areas. Such an approach has the benefit of sampling the network in a controlled and purposeful manner, allowing comparative analysis of specific areas of interest within a network. Subsequent geometric and topological analysis links each digitally mapped fracture to the sample area by a unique identifier. A full area sampling (Fig. 3B) creates a polygon that covers the entire network region using an automated minimum bounding box envelope. This allows users to quickly sample the entire fracture network in an efficient approach.

Line Sampling

Although the toolkit is largely based on areal sampling, we also provide a one-dimensional line sampling approach (Figs. 3C and 3D), which uses a linear polyline feature to sample a network at each intersection with a fracture. This can be useful when analyzing spatial distributions and spacing of individual fracture sets, although it should be noted that it is important to draw the sample line perpendicular to the trend of the fracture set to avoid under sampling (Terzaghi, 1965). Distance along the sample line is calculated using a modified “centerline calculation” by Nyberg et al. (2015); this calculation determines the polyline start coordinates and then cumulatively sums the distances between each intersected fracture. To create a polyline feature as an input to the line sampling method, two options are available. A manual approach may be used to define a specific line sample (Fig. 3C). Alternatively, a line grid method (Fig. 3D) will take the boundary of the fracture network to automatically create a regularly spaced set of parallel polylines at a user-specified spacing and angle. Such a line grid allows for multiple, equally spaced samples to define spatial trends within a data set.

Network Grid Sampling

In order to objectively and consistently sample spatial variations throughout a network, we have implemented an automated regular grid that subsamples

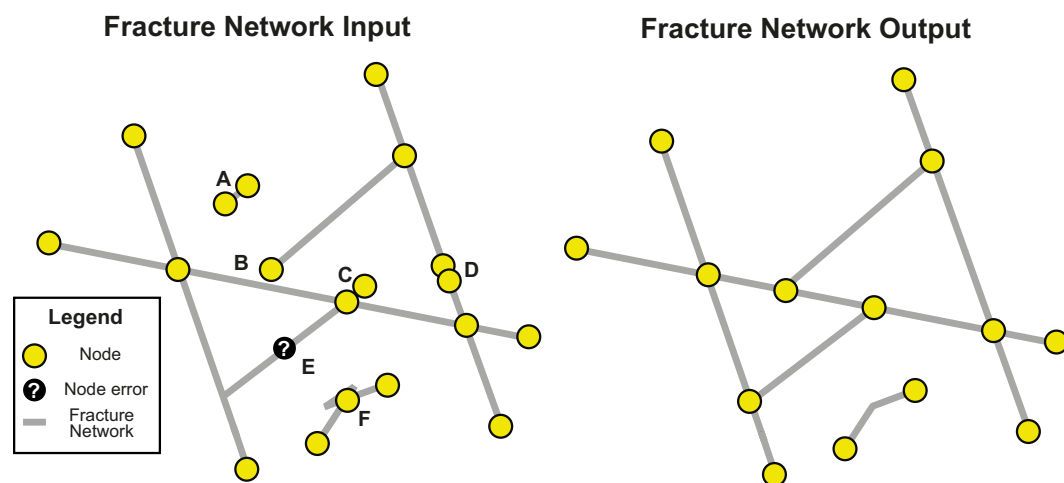


Figure 2. Common topological errors during digitization of a fracture network, producing a network that is topologically inconsistent; and the repaired fracture network that is output from the “repair network” tool. The errors and reparations considered by the tool include: (A) removing erroneous short isolated fracture lines; (B) extending and snapping fracture lines to existing fractures; (C) trimming and snapping fracture lines to existing fractures; (D) merging and snapping offset fracture lines; (E) removing overlapping fracture lines and/or merging fragmented fracture lines that lead to inconsistent node counts; and (F) removing circles within fracture lines.

the entire fracture network in squares of specified size. The network grid sampling method (Figs. 3E and 3F), uses the known extent of the interpretation boundary (Fig. 3E) to define a square grid of polygons starting from the lower left corner by a user’s specified parameters of width and height. Only those grids that are within the interpretation boundary are created. This subsampling allows for a quantitative analysis of topological and geometric variation throughout a fracture network. However, given the granularity of the subsampling spacing, it is possible that the underlying trend is removed. To address this problem, an additional optional parameter will define the centroid point within each gridded subsample area and extract the topological or geometric attributes within a user-defined search radius (Fig. 3F). The search radius will only extend to the interpretation boundary to ensure that both topological and geometric parameters have minimal influence from edge effects. It should be noted that the choice of radius (i.e., circle size) should take into consideration the spatial distribution of the fractures in order to reduce sampling effects (Rohrbaugh et al., 2002). A unique identifier then links each subsample grid area to each point and search radius. This allows the original square grid of polygons to display properties of the fracture network as contour grids while having the benefit of providing a greater search area to increase the granularity of the analyses.

■ GEOMETRIC ANALYSIS

The NetworkGT toolbox consists of a set of tools designed to analyze the orientations, sets, lengths, intensity, and spatial heterogeneity or spacing of the fractures within the network. The tools process the spatial data associ-

ated with each fracture polyline to create a variety of quantitative graphs that are traditionally used in fracture network analysis, including length-weighted rose diagrams and length-frequency plots. When analyzing different sample areas, multiple graphs will be produced and are linked to each sample area by a unique identifier. Below we describe each geometry tool following a suggested workflow.

Defining Fracture Orientations

Orientation analysis is often the first step in assessing a fracture network in order to define the main fracture trends and thus identify fracture sets (Fisher, 1993). A “rose diagram” tool classifies fracture lines or branches into bins based on their azimuth angle, as defined by the start and end point coordinates of a polyline, grouping the fractures into user-specified bin sizes (e.g., 10° intervals, Fig. 4). The tool produces a rose diagram that plots the fracture frequency within each bin as a percentage of the total count. The rose-diagram tool offers the option to weight the rose diagram by a parameter, such as length or displacement. In this case, the sum of the weighted parameter within each bin is plotted as a percentage of the total sum of the weighted parameter for the sampled network.

A rose diagram can help to visualize and define sets of fracture orientations within a fracture network; for example, the data in Figure 4 indicate a bimodal distribution with NE- and NW-trending fracture sets. The “sets” tool can subsequently be used to categorize the fractures by their identified sets and add this attribute to each fracture line or branch within the network. This is achieved by defining the orientation of each fracture polyline, using their start and end

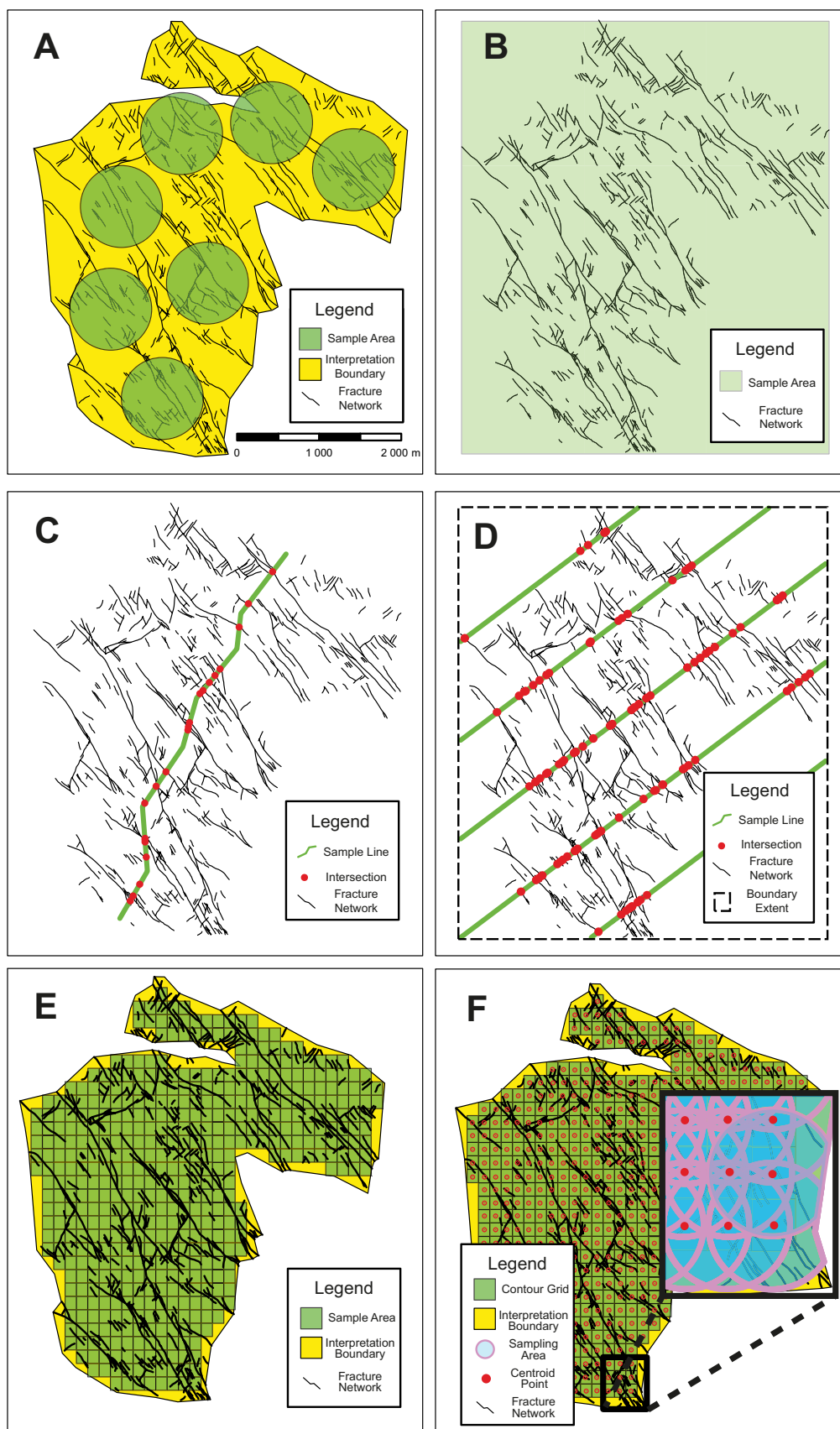


Figure 3. Sampling strategies provided by the NetworkGT toolbox demonstrated on a fracture network offshore NW Devon, United Kingdom. (A) Manual polygon sampling approach to subsample areas of interest within the network by creating arbitrary polygons. (B) Full area sampling approach that envelops the entire fracture network by creating a polygon based on the spatial extent of the fractures within the network. (C) Manual line sampling approach creating an arbitrary polyline across the network that samples each intersecting fracture. (D) Grid line sampling approach creating a series of user specified spaced and angled, parallel sampling lines (example shown has spacing and angle of 1000 m and 53°, respectively) within the boundary of the original fracture network. (E) Sampling as a series of user-specified, equally spaced grid polygons (example has grid of 100 m x 100 m) that are completely within the extent of the interpretation boundary to create a contour grid. (F) Application of the centroid point of each contour grid in (E) and samples within a user-specified radius (example radius is 250 m) to the extent of the interpretation boundary.

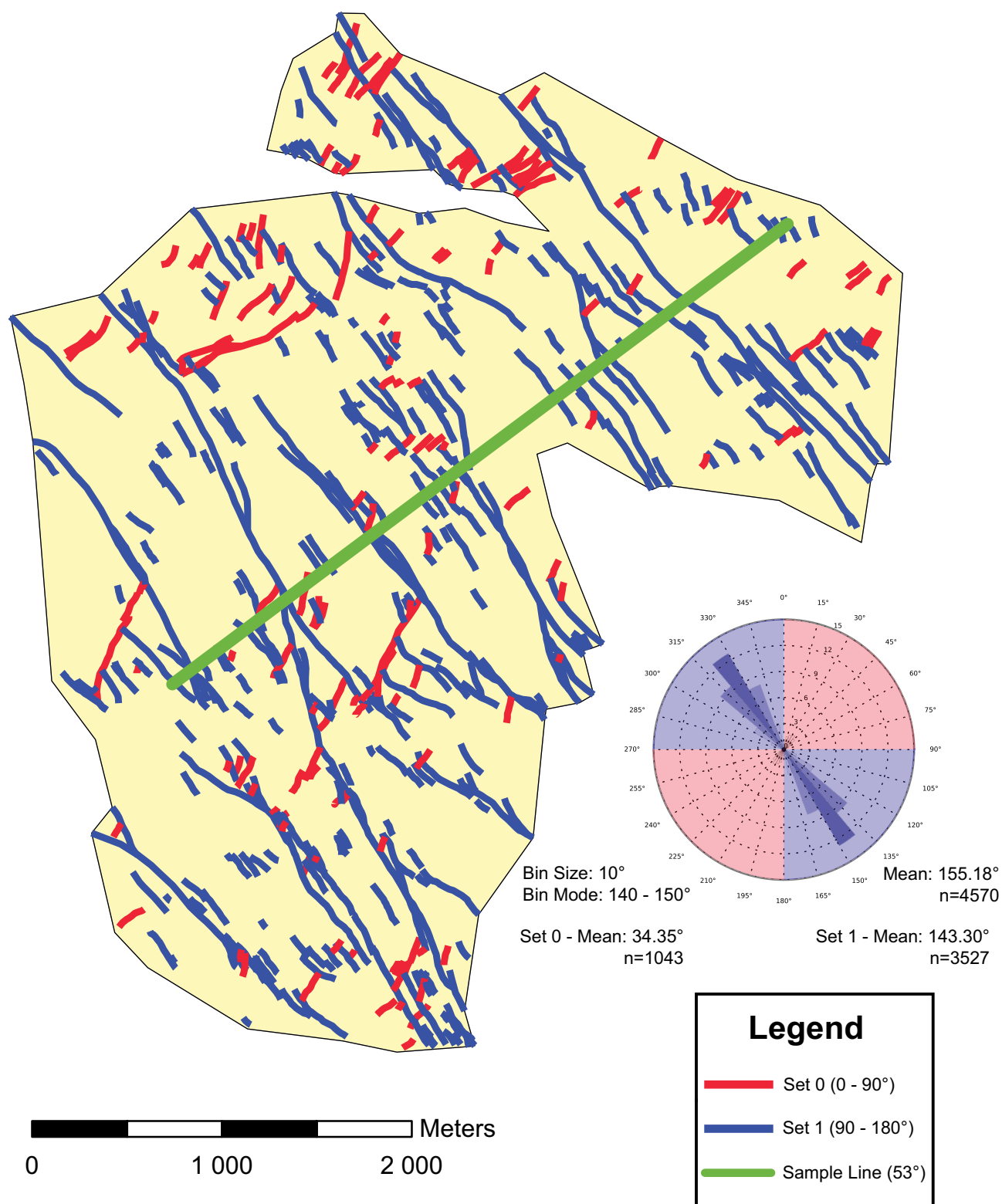


Figure 4. Orientation analysis of the fracture network offshore NW Devon, United Kingdom. A length-weighted rose diagram with 10° bins indicates a mean fracture orientation of 155° and a bin mode between 140° and 150°. It illustrates a minor fracture set (0) and major fracture set (1) with mean orientations of 34° and 143°, respectively. Fracture orientations are calculated from the individual segment components of fracture lines to capture the complete orientation variability. The fracture trace map classifies the fractures into the two fracture sets based on their range of orientation; set 0 ranges from 0 to 90° (red), and set 1 ranges from 90° to 180° (blue). A linear sample line (green) is overlain perpendicular to set 1 (53°), which is used in Figure 5A to sample spatial heterogeneity of the fracture set.

point coordinates, and then grouping them sequentially into user-defined sets ranging from 0° to 180°. These sets can then be displayed differently on the fracture trace map (Fig. 4) allowing visualized comparison of the spatial variability and topology of the fracture sets. Furthermore, the tool will summarize the mean orientation and mode of the binned orientations for the fracture network or fracture network sets, which may be used to assess the perpendicular azimuth in line sampling approaches (see below).

Assessing Spatial Heterogeneity

Line samples perpendicular to the azimuth of a fracture set can be applied to determine fracture frequency (intensity), spacing, and spatial heterogeneity (Fig. 5A). Spatial heterogeneity is important because it can give an indication of the organization of the fractures and whether they are distributed or localized (Putz-Perrier and Sanderson, 2008, 2010; Nixon et al., 2014). The “spatial

heterogeneity” tool uses a method that directly quantifies spatial heterogeneity following Putz-Perrier and Sanderson (2008). The tool determines the distance to each fracture along a line sample and plots the distance against normalized cumulative frequency (Fig. 5A). Optional parameters allow users to assess specific fracture sets or types and/or to plot line sampling distance against a normalized cumulative weighted attribute. The spatial heterogeneity (V) of the plot is quantified by summing the maximum deviations above and below a uniform distribution, D^+ and D^- , respectively (Fig. 5; Putz-Perrier and Sanderson, 2008). Values of V will range from 0 to 1 representing more homogenous or heterogeneous distributions, respectively.

Fracture-Length Distributions

Determining frequency distributions of fracture attributes such as fracture length is common practice in the analysis of fractures (e.g., Gillespie et al.,

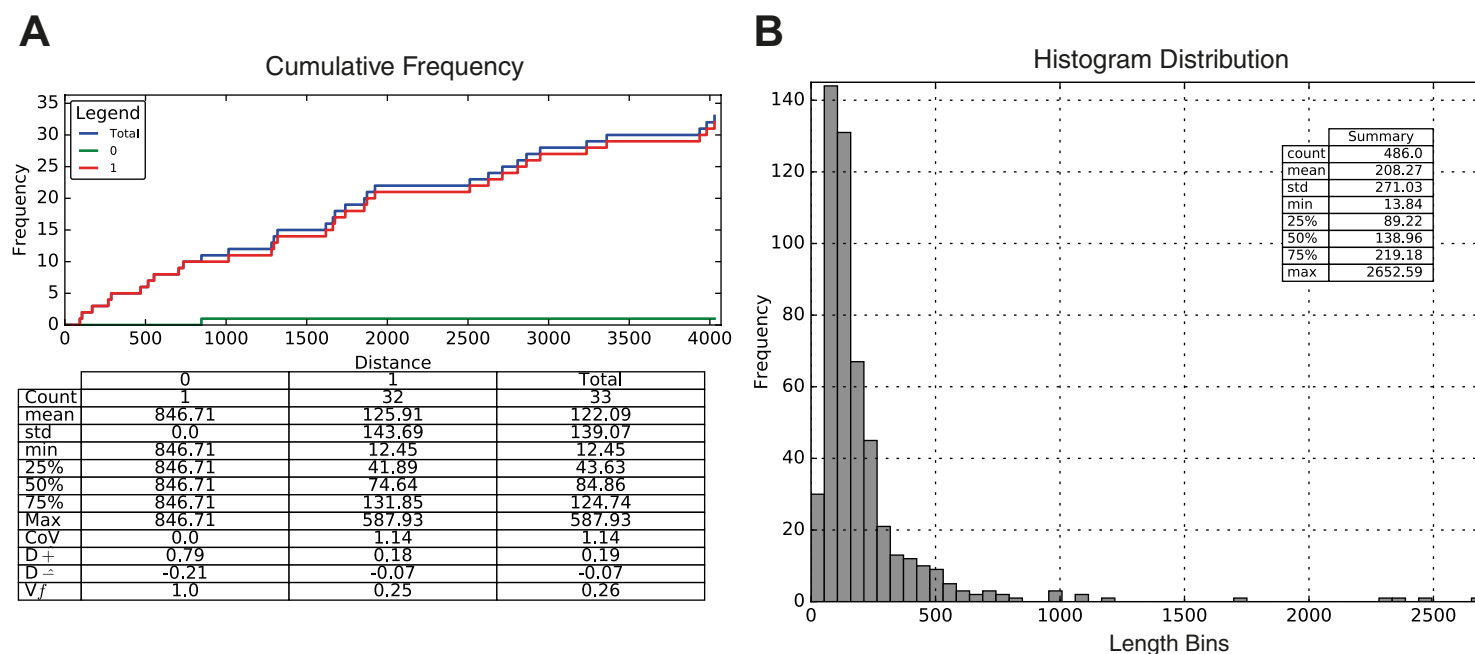


Figure 5. Outputs of the geometry aspect of the NetworkGT toolbox based on the fracture network in Figures 3 and 4. The spatial heterogeneity of fractures along the linear sample line in Figure 4 is illustrated in (A), which shows a plot of distance along sample line versus cumulative frequency and a table of statistical information. Furthermore, the plot and table are subdivided by sets (sets 0 and 1 from Fig. 4) to display spatial trends of different groups of fracture orientations. The heterogeneity measure of fracture set 1 ($V_f = 0.25$) indicates a relatively homogenous distribution of fractures along this sampling line (see text for explanation of heterogeneity measure). (B) Histogram distribution of fracture lengths, grouped into 50 bins, for the entire fracture network and an inset table of statistics summarizing the distribution.

1993; Bonnet et al., 2001; Kim and Sanderson, 2005; Torabi and Berg, 2011). The NetworkGT toolkit provides a number of tools for visualizing and assessing frequency distributions of selected fracture attributes. A simple “histogram” tool enables a quick distribution analysis producing a histogram, with a user-specified number of bins for fracture properties (fracture length; Fig. 5B). Another distribution analysis tool will produce a table of statisti-

cal values and a series of cumulative frequency plots, allowing the user to determine frequency distribution trends (Fig. 6). Trends in the distribution of such attributes can be identified and described as negative exponential, log-normal, or power-law (Bonnet et al., 2001). These include standard deviation plotted against log (length); log (cumulative percentage) plotted against length; and log (cumulative percentage) plotted against log (length).

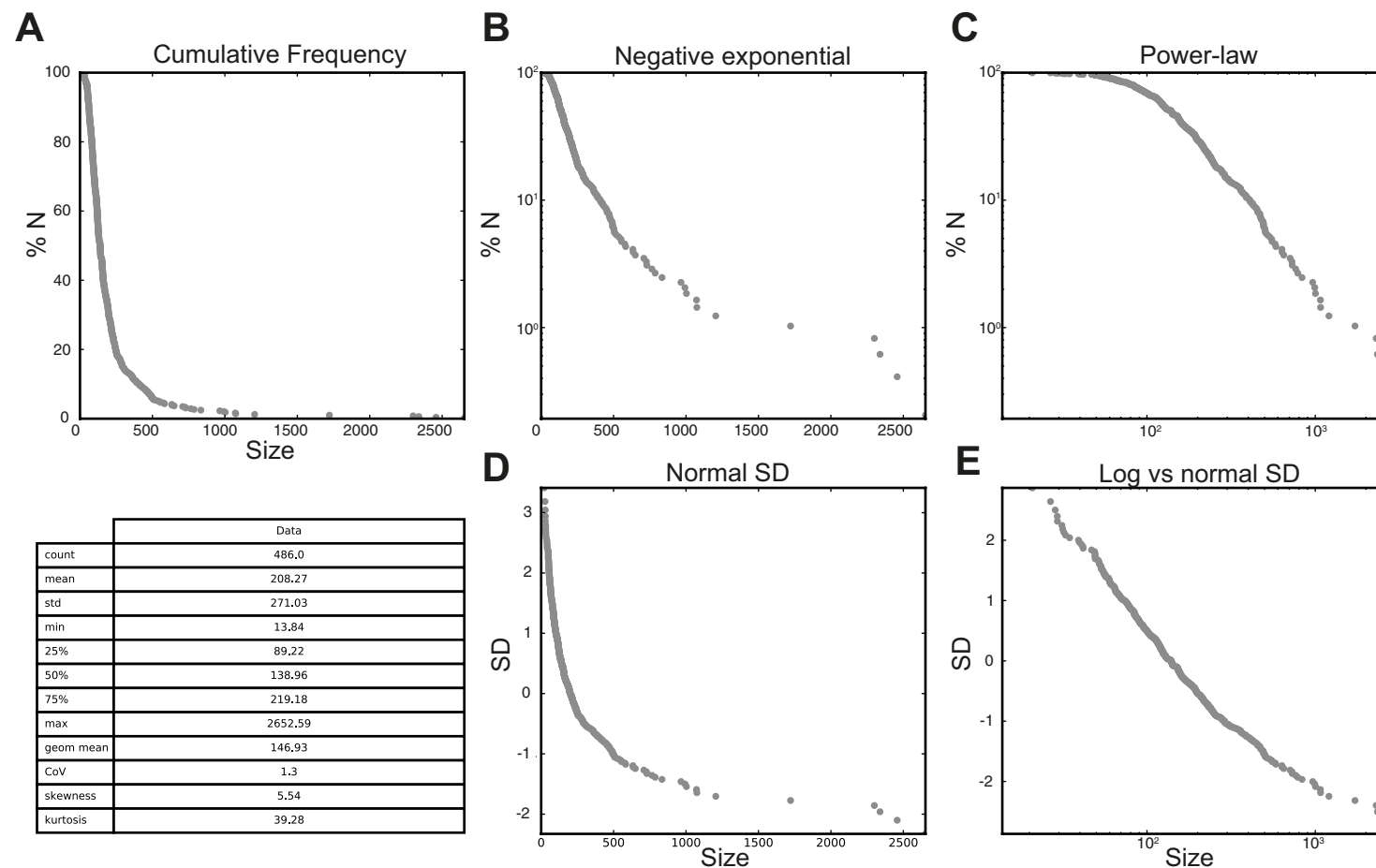


Figure 6. Distribution analysis of fracture lengths using a series of cumulative frequency plots and a table of statistics for the entire fracture network offshore NW Devon, United Kingdom (Fig. 4). Plots from upper left to bottom right are: (A) Cumulative percentage plotted against length; (B) log (cumulative percentage plotted against length); (C) log (cumulative percentage) plotted against log (length); (D) standard deviation plotted against length; and (E) standard deviation plotted against log (length). A straight line on (B), (C), or (E) would indicate either a negative exponential, power-law, or log-normal distribution; however, it is important that the user recognizes and evaluates potential of sampling biases such as censoring or truncation when interpreting the plots. The data indicate a power-law distribution for the fracture lengths offshore NW Devon.

A straight line distribution on either plot would indicate a log-normal, negative-exponential, or power-law distribution, respectively; however, the user is advised to be aware of sampling biases when interpreting distributions (e.g., Pickering et al., 1995). Both distribution tools within the NetworkGT package will optionally provide outputs based on specified grouping parameters, such as fracture set, as well as a weighted parameter, such as fracture displacement, for comparative analysis.

■ TOPOLOGICAL ANALYSIS

Recent publications have established the application of topology to fracture networks, developing useful topological parameters to analyze and char-

acterize networks (e.g., Manzocchi, 2002; Nixon, 2013; Sanderson and Nixon, 2015). In two dimensions, the topology of a fracture network consists of lines, nodes, and branches between nodes (Fig. 7A). Nodes are divided into isolated (I) nodes and connecting nodes (X and Y nodes) (Manzocchi, 2002; Sanderson and Nixon, 2015). Because the ends of branches are marked by nodes, we can classify branches into three topological groups: I-I, I-C, and C-C branches (Sanderson and Nixon, 2015). The number and proportion of different node and branch types can be used to simply calculate further statistics that quantify and assess the connectivity, clustering, and block proportions of a fracture network (i.e., Sanderson and Nixon, 2015). However, the manual extraction of topological data is time consuming and subject to error; thus, in this section, we outline how the NetworkGT toolkit may be used to automatically extract and analyze topological data. We describe the algorithms behind a number of

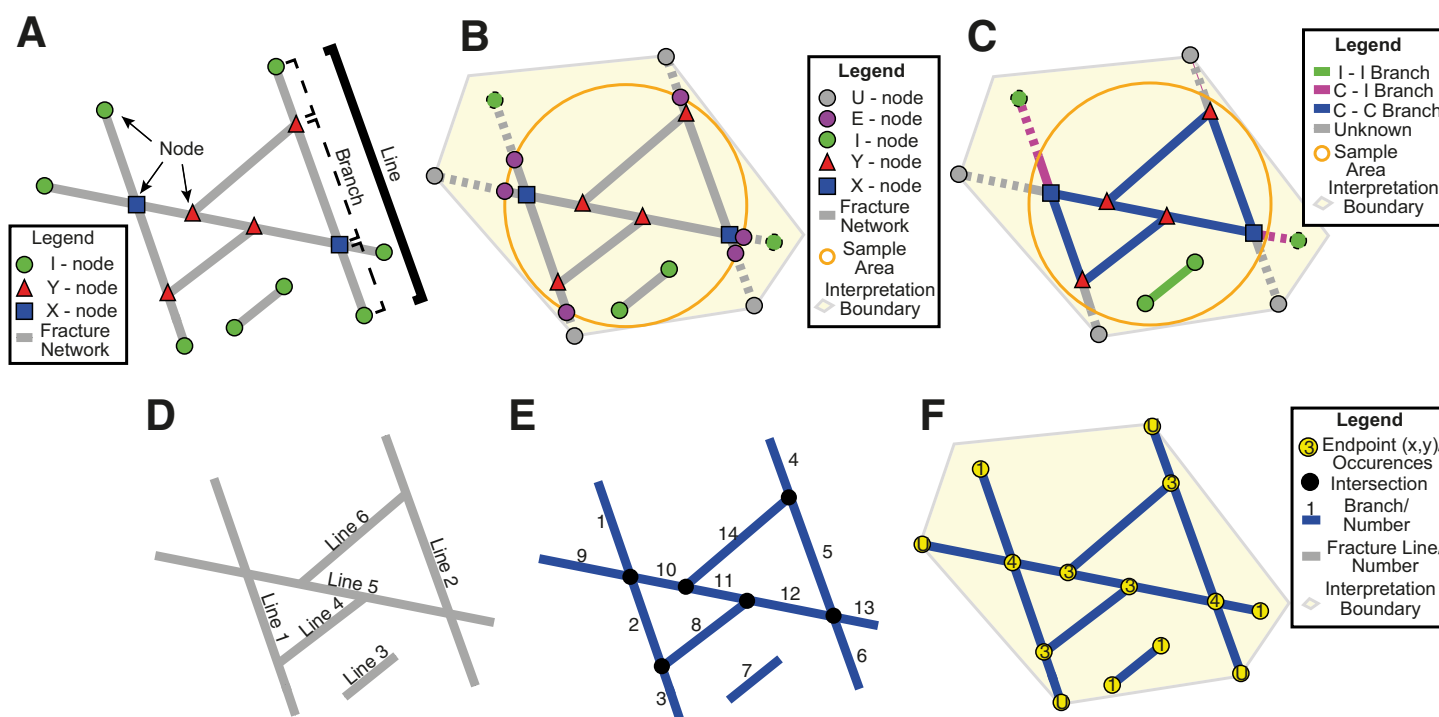


Figure 7. In two dimensions, the topology of a fracture network is considered in terms of lines, nodes, and branches as illustrated in (A). The nodes of the fracture network are classified as isolated (I) nodes or connecting (Y or X) nodes. Given a sample area and interpretation boundary, (B) additional edge (E) nodes and unknown (U) nodes are recognized when a fracture intersects the perimeter of the sample area or the interpretation boundary, respectively. Branches are classified based on the node information both within and outside of the sample area, (C), as isolated branches (I-I), singly connected branches (C-I) or doubly connected branches (C-C). Unknown branches are also identified where a branch intersects the interpretation boundary. The extraction of nodes and branches is achieved by inputting a topologically consistent two-dimensional digitized fracture network of lines and splitting the fracture lines at their intersections, as illustrated in (D) and (E). The algorithm identifies unknown nodes at the interpretation boundary and other node types based on the number of node occurrences at each fracture tip and/or intersection (I = 1, Y = 3, X = 4) as illustrated in (F).

tools presenting them in a logical workflow. Again, each tool can be applied to multiple sample areas simultaneously with results linked to sample areas by unique identifiers.

Extraction of Nodes and Branches

The “node and branch” tool identifies and extracts the different node (I, Y, and X) and branch (I-I, I-C, and C-C) types from a network of fracture polylines within a sample area polygon (Figs. 7B and 7C). It also identifies edge (E) nodes, where a fracture intersects the sample area, and unknown (U) nodes, where a branch intersects the interpretation boundary and its extent is therefore unknown (Figs. 7B and 7C).

The tool works by considering geospatial relationships between nodes, branches, and lines. Firstly, the branches within each fracture polyline are extracted as a new set of polylines, calculated by splitting the fracture polylines at their intersections to one another (Figs. 7D and 7E). The coordinates of the endpoints of each branch polyline are then stored in a point graph noting the number of occurrences of each specific coordinate (Fig. 7F). Because I nodes are associated with a single branch, whereas Y nodes and X nodes connect

three and four branches, respectively, the occurrences of each endpoint coordinate identify the node type (I = 1, Y = 3, X = 4; Fig. 7F). The coordinates at which the branches intersect the interpretation boundary are also stored in the point graph and are identified as U nodes (Fig. 7F).

Once the node types and coordinates of each branch endpoint have been defined (Fig. 8A), the algorithm classifies the branch polylines as either I-I, C-I, C-C, I-U, C-U, or U-U (Fig. 8B). The geospatial location of each branch is tested against all sample areas and linked via a sample identifier. This ensures that all branches and nodes are calculated, even in circumstances where sample areas overlap one another, which is particularly useful in a network grid sampling method (Fig. 3F) when duplicate measurements may be present but are part of different sample areas.

If the entire length of a branch polyline (Fig. 8C) is geospatially located within a sample area, then the branch is given a weighting of 1 (Fig. 8C). However, when a branch polyline is only partially within a sample area, an additional set of steps is applied. The algorithm will split such branch polylines at the perimeter of the sample area polygon and test if either branch endpoint lies within the sample area. In circumstances where one endpoint of a branch is outside the sample area, the branch is given a weighting of 0.5 to indicate that it is partially within the sample area (Fig. 8C). In a situation where both

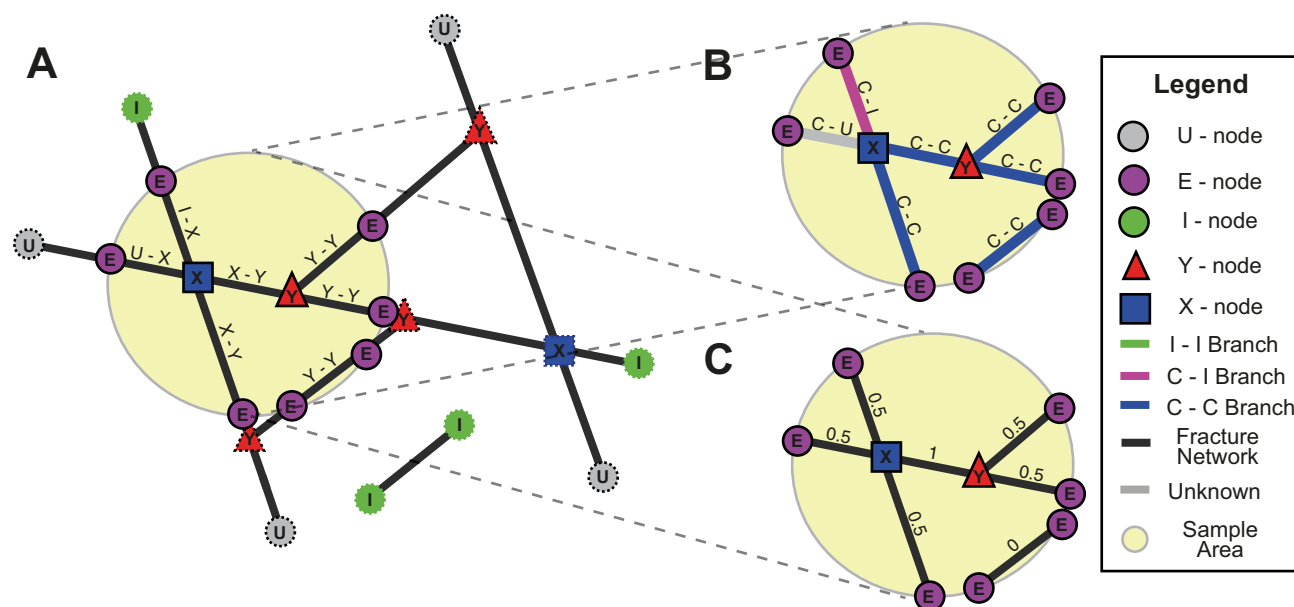


Figure 8. (A) Illustrates the nodes classified within a sample area, based on the number of node occurrences (Fig. 7F) and edge nodes that intersect the sample area. The different node types are subsequently applied to classify branches within each sample area in (B). Each branch is associated with a weight of either 0, 0.5, or 1, as shown in (C), indicating whether the branch passes through the sample area, partially leaves the sample area, or is completely within the sample area, respectively.

endpoints of the branch are outside the sample area, the branch is given a weighting of 0 to indicate that the branch passes through the sample area (Fig. 8C). In both cases, the intersected portion (Figs. 8B and 8C) of the original branch (Fig. 8A) that lies within the sample area is subsequently kept and classified according to its original branch classification scheme (Fig. 8B). The intersection coordinates with the sample area perimeter are stored in the node point graph as edge (E) nodes.

The resultant feature class of branch polylines contains branch and associated sample identifier along with the length of the branch within the sample area, its classification, and weighting. The information stored in the node point graph (coordinates, associated sample identifier, and node classification) is used to create an additional feature class of nodes, discarding any duplicate points with the same sample identifier.

Characterization of Network Topology

Branch and node feature classes allow visualization of a network's topology, as illustrated in Figure 9, and can be used as input for further characterization and analysis. An array of topological measures and parameters can be calculated with the "topology parameters" tool using the node and branch counts in combination with the branch lengths. These include measures of fracture abundances and a number of dimensionless parameters that describe the connectivity of a network, such as the average connections per branch and the dimensionless intensity, and can be linked to percolation thresholds (e.g., Manzocchi, 2002). Table 1 summarizes these parameters with a short description; however, for further derivation, see Sanderson and Nixon (2015). The "topology parameters" tool adds this information to each sample area polygon and offers an optional spreadsheet output.

The number of different I, Y, and X nodes and I-I, I-C, and C-C branches extracted from a sample area can be illustrated in a series of ternary plots. This is handled within the "topology plot" tool of the NetworkGT toolkit; this tool utilizes a Python ternary module (Harper et al., 2015) to map the different nodes and branches as proportions (Figs. 9B and 9C). The different ternary plots also include contours that indicate the number of connections per branch, with values ranging from 0 to 2, and thus are useful for characterizing the topology and assessing connectivity.

Assessment of Clusters and Blocks

Clustering and block analyses provide another aspect of the NetworkGT toolkit for the user with an automated means of extracting numbers, sizes, and spatial distributions of clusters and blocks within a fracture network. Such analyses provide insight into the fluid-flow behavior of a network with large spanning clusters, potential pathways, and/or barriers for fluid flow (Adler and Thovert, 1999). Clusters are extracted using an algorithm that iterates

over every fracture or branch, grouping connected polylines and assigning unique cluster identifiers for the entire fracture network (Fig. 10A) or for the sample area (Fig. 10B). If the branches are used as the input to the "clustering" tool, additional options may be used to characterize connected clusters and statistically summarize the branch types (i.e., C-I, C-C, and C-U branches) and lengths that compose them. By extracting the statistics of each cluster, the user can assess the connected parts of a network and easily identify the largest clusters.

Spatial distributions and sizes of internal blocks within a fracture network are important when quantifying the amount of fluid-rock interaction or potential compartmentalization. The NetworkGT toolkit provides the user two methods for quantifying the number and sizes of blocks within a sample area. The "identify blocks" tool uses the surrounding fracture network to extract and identify the true distribution and size of blocks. This first method utilizes the original polylines of the fracture network and converts those lines to polygons to determine any internal blocks within the network (Fig. 10A). The algorithm will subsequently iterate through all sample areas and determine any overlap with the previously identified blocks. A block count parameter will count all overlapping blocks in the sample area, and an intersected block count will count all blocks that leave the sample area (Fig. 10A). Further information associated with the overlapping block areas such as minimum, mean, and maximum sizes are then recorded to each sample area.

In the case where the mapped spatial extent of a fracture network may be incomplete or limited (e.g., well-bore imagery, cores, and limited outcrops), we provide a novel "block analysis" that allows the user to extrapolate block potential of the surrounding network. For a given sample area, the algorithm quantifies the total number of clusters (K_i); number of clusters that intersect the perimeter (K_j); number of nodes (N), number of edge nodes (N_e); and branches (B) that define those clusters. The algorithm excludes all information outside of the sample area. The tool then provides block calculations following Euler's theorem, where the number of whole blocks (W_b) within a sample area are related to the total number of nodes, branches, and clusters by:

$$W_b = B - N + K_i.$$

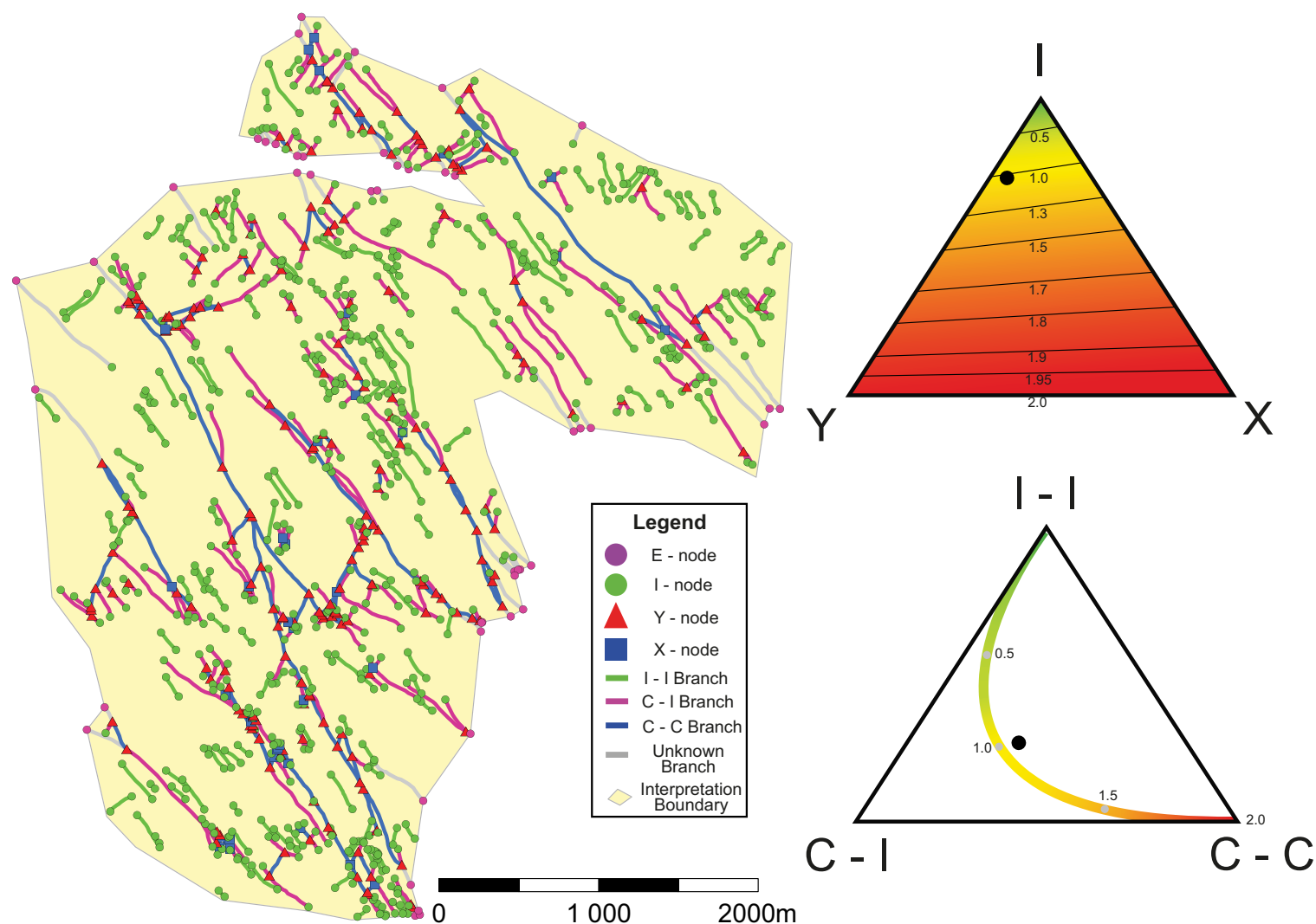
The "block analysis" will also determine the potential number of half blocks (H_b) that lie partially within the sample area given by:

$$H_b = (N_e - K_j + 1)/2, \text{ if } K_j > 0$$

$$H_b = 0, \text{ if } K_j = 0.$$

By summing the number of whole blocks and half blocks, the tool defines the number of theoretical blocks ($T_b = W_b + H_b$) for the sample area (Fig. 10F). This can be particularly useful when assessing block sizes providing an average block size for the network by dividing the number of theoretical blocks by the sample area (i.e., T_b/A).

Figure 9. The fracture network offshore NW Devon, United Kingdom, classified into nodes and branches based on the methodology in Figures 7 and 8. The upper right shows the fracture network's node classification plotted on an I, Y, and X ternary diagram, and the lower right shows the branch classification plotted on an I-I, C-I, and C-C ternary diagram. The lines contoured onto the ternary plots indicate thresholds for number of connections per branch ranging from 0 to 2.



SPATIAL VISUALIZATION OF NETWORK PROPERTIES

Automated extraction of geometric and topological properties for multiple subsampled areas provides a means by which to efficiently analyze spatial variability in a fracture network. The network grid sampling strategy provides a framework for visualizing these spatial variations by creating a densely spaced grid. Each grid cell shares a centroid point with an associated circular sample

area of specified radius (Fig. 3F). All the extracted topological and geometric information are related to each sample area by unique identifiers; therefore, every grid polygon has a number of calculated parameters and properties stored as associated network attributes. Thus, we can create high-resolution, geospatially referenced contour grids that map and illustrate spatial variations of important network properties (e.g., fracture abundances, connectivity, block sizes, and distributions) throughout a fracture network.

TABLE 1. SUMMARY OF PARAMETERS GATHERED BY THE “TOPOLOGY PARAMETER” AND “BLOCK ANALYSIS” TOOLS FOR THE TOPOLOGICAL ANALYSIS OF FRACTURE NETWORKS

| Topology parameter tool | | |
|---|--|--|
| Parameter | Calculation | Description |
| Area (A) | A | Area of sample region |
| Number of nodes (N_n) | $N_I + N_Y + N_X$ | Count of I, Y, and X nodes |
| Number of connections (N_C) | $N_Y + N_X$ | Count of X and Y nodes |
| Number of edge nodes | N_E | Count of E nodes |
| Number of branches (node calculation) (N_B) | $N_I + 3N_Y + 4N_X$ | Number of branches calculated from nodes |
| | 2 | |
| Number of lines (N_L) | $N_I + 2N_Y$ | Number of lines calculated from nodes |
| | 2 | |
| Connect/line (C_L) | $\frac{2(N_Y + N_X)}{N_L}$ | Connections per line |
| | N_L | |
| Connections/branch (C_B) | $\frac{3N_Y + 4N_X}{N_B}$ | Connections per branch |
| | N_B | |
| Total trace length (ΣL) | ΣL | Sum of all branch lengths |
| Average line length (L_C) | $\Sigma L / N_L$ | Average line length |
| Average branch length (B_C) | $\Sigma L / N_B$ | Average branch length |
| Connecting node frequency ($N_C \text{ km}^{-2}$) | N_C / A | Frequency of connecting nodes within the sample area |
| Branch frequency (B_{20}) | N_B / A | Frequency of branches within the sample area |
| Line frequency (P_{20}) | N_L / A | Frequency of lines within the sample area |
| 1D intensity (P_{10}) | $\frac{N_E}{2\pi r} \cdot \frac{\pi}{2}$ | Intensity fractures from circular line sample where r is the radius of the sample area |
| | $\Sigma L / A$ | Intensity of fractures within a sample area |
| 2D intensity (P_{21}) | $\Sigma L / A$ | Intensity of fractures within a sample area |
| Dimensionless intensity (B_{22}) | $P_{21} \cdot L_B$ | Dimensionless intensity is the product of the average branch length and intensity |
| Number of branches (branch calculation) (N_B) | $N_{CC} + N_{CI} + N_{II}$ | Count of C–C, C–I, and I–I branches |
| Block analysis tool | | |
| Parameter | Calculation | Description |
| Number of clusters (K_{ij}) | K_{ij} | Count of clusters in sample area |
| Number of intersecting clusters (K_i) | K_i | Count of clusters intersecting sample perimeter |
| Number of branches (block calculation) (B) | $N_I + N_E + 3N_Y + 4N_X$ | Number of branches calculated from nodes (including E nodes) |
| | 2 | |
| Number of nodes (block calculation) (N) | $N_I + N_E + N_Y + N_X$ | Count of I, E, Y, and X nodes |
| Number of whole blocks (W_b) | $B - N + K_{ij}$ | Number of whole blocks within sample area |
| Number of half blocks (H_b) | $N_E - K_i + 1$ | Number of potential blocks that are partially within the sample area |
| | 2 | |
| Number of theoretical blocks (T_b) | $W_b + H_b$ | Sum of the number of whole blocks and number of half blocks |
| Theoretical block size | T_b / A | Average area of a theoretical block |

We illustrate the quantitative efficiency of contour grid mapping using the fracture network of Nixon et al. (2012) and applying a 100 m × 100 m network grid sample, where each grid cell has an associated circle sample with a 250 m radius, creating 1326 sample areas over the study region (Fig. 3F). By inputting only the interpretation boundary, the digitized fracture network, and the network grid sample into the “node and branch” tool, a total of 16,777 nodes and 16,881 branches were identified and extracted, excluding an additional 8970

edge and/or unknown nodes and 736 unknown branches. It would be impractical to obtain this extracted information using manual alternatives. Further parameters and properties (e.g., Table 1) can then be calculated and mapped as contour grid plots, as illustrated in Figure 11 for the fracture intensity, connecting node frequency, connections per branch, and number of theoretical blocks. Implementation in a geospatially referenced GIS environment provides an array of powerful user-designed visualization options.

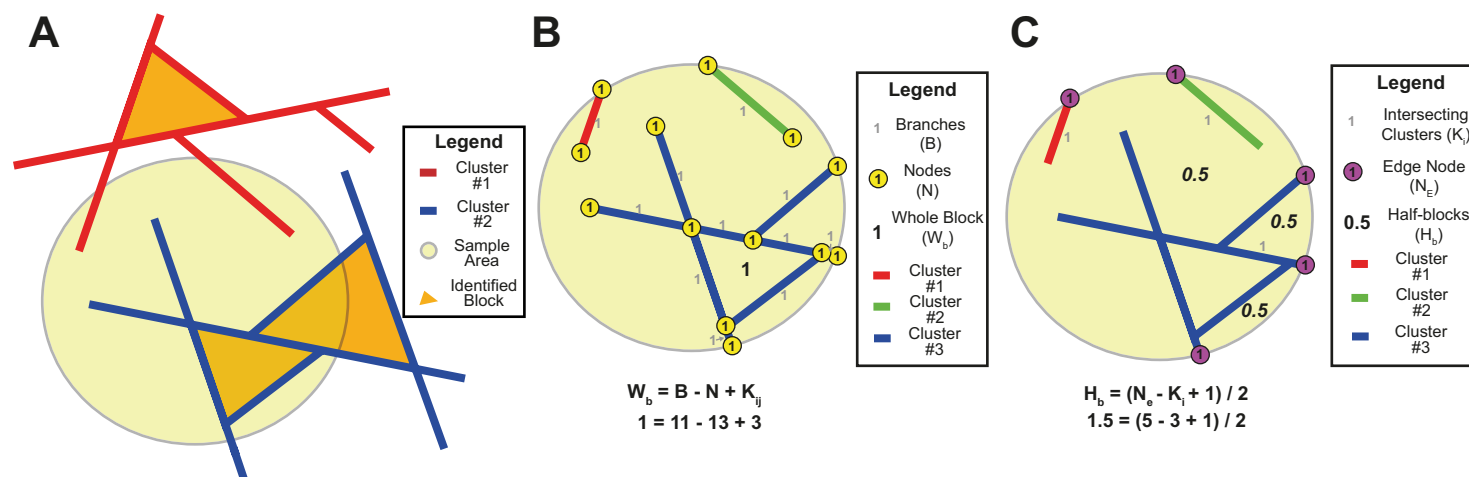


Figure 10. Various techniques for classifying clusters and blocks within a fracture network. In (A), clusters are defined based on the entire fracture network and statistically summarized by the different branch types within each cluster. The “block identifier” tool identifies the actual geospatial distribution of blocks for the entire network, subsequently defining the number of whole blocks and partial blocks within the sample area shown in (A). In (B) and (C), clusters are defined for each given sample area, and the “block analysis” tool uses the numbers of branches (B), nodes (N), edge nodes (N_e), clusters (K_i), and intersecting clusters (K_i) to calculate the number of whole blocks (W_b), half blocks (H_b), and theoretical blocks (T_b) for the sample area. See Table 1 and text for further explanation of calculations.

Contour grids provide regular and uniformly sampled grids that contain several parameters describing network properties (Table 1). Multiple contour grids can be used to visually compare the properties of different fracture populations within a network (e.g., different fracture sets) or to evaluate network properties as a network develops. In addition to providing a visual comparison, different contour grid plots can be input into a “topology calculator” tool to determine, for instance, the difference, mean, range, and standard deviation between multiple contour grids. This is achieved by ensuring that the grid polygons and their unique sample identifiers are the same for each contour grid that is analyzed (Fig. 12A). Furthermore, a time series of multiple contour grids can be created, thus providing a means to visualize the absolute change or differences in the parameters of Table 1 with time as a fracture network develops and evolves (Fig. 12B).

CONCLUSIONS

This paper has presented NetworkGT, a new open-source ArcGIS toolbox comprising a suite of customized tools dedicated to the sampling, analysis, and spatial mapping of geometric and topological attributes of two-dimensional fracture networks. The incorporation of topological parameters is a significant advance on existing analysis tools. Different aspects of the tool-

kit and the algorithms behind each tool have been described and applied to a natural fracture network, from NW Devon, United Kingdom, in a repeatable workflow that follows: (1) selection of an appropriate sampling strategy; (2) geometric analysis; (3) topological analysis; and (4) spatial visualization of network properties. The tools are based on traditional and novel methods, brought together in a GIS framework to provide an objective and efficient characterization and quantitative analysis of a fracture network. Highlights of the toolbox include:

- An aid to repair digitized fracture networks so that they are geospatially and topologically consistent, particularly useful for automatically digitized fracture maps;
- A variety of one- and two-dimensional sampling strategies (e.g., line, areal, and grid sampling), including systematic methods for sampling the spatial variations within a fracture network;
- Extraction and analyses of geometric attributes including a number of graphs and plots that describe length, orientation, and spatial heterogeneity statistics;
- Automated extraction and calculation of topological information including nodes, branches, and associated statistics that describe fracture abundances and connectivity;
- Automated identification and extraction of clusters and blocks as well as associated statistics for assessing their numbers and sizes;

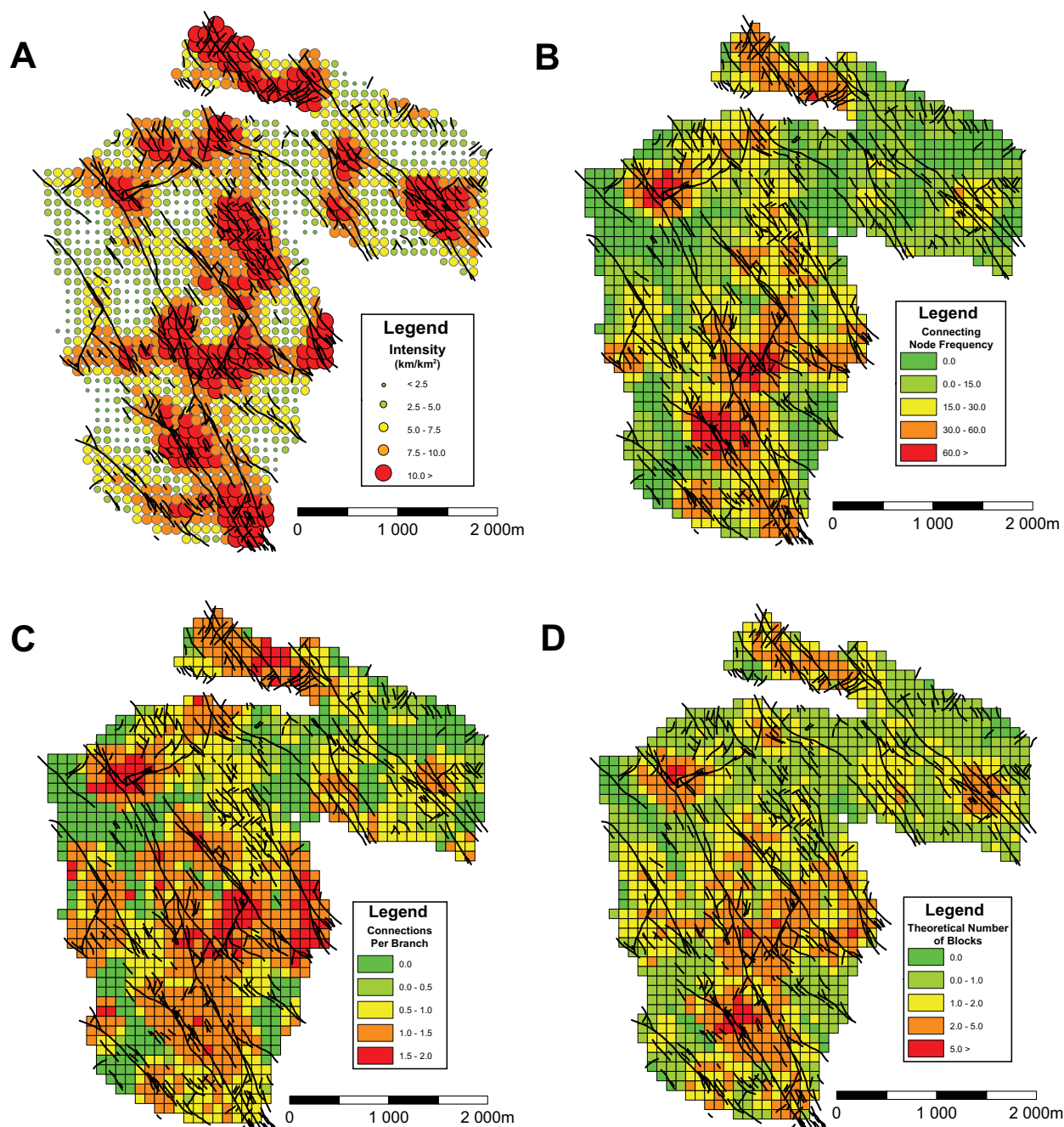


Figure 11. The spatial visualization of four fracture network properties, including: (A) fracture intensity; (B) connecting node frequency; (C) connections per branch; and (D) number of theoretical blocks. These properties are based on a 100 × 100 m contour grid with a specified search radius of 250 m (e.g., Fig. 3F) and illustrate spatial variations in fracture abundances, connectivity, and block distribution. Any parameter from Table 1 can be illustrated using this contour grid methodology.

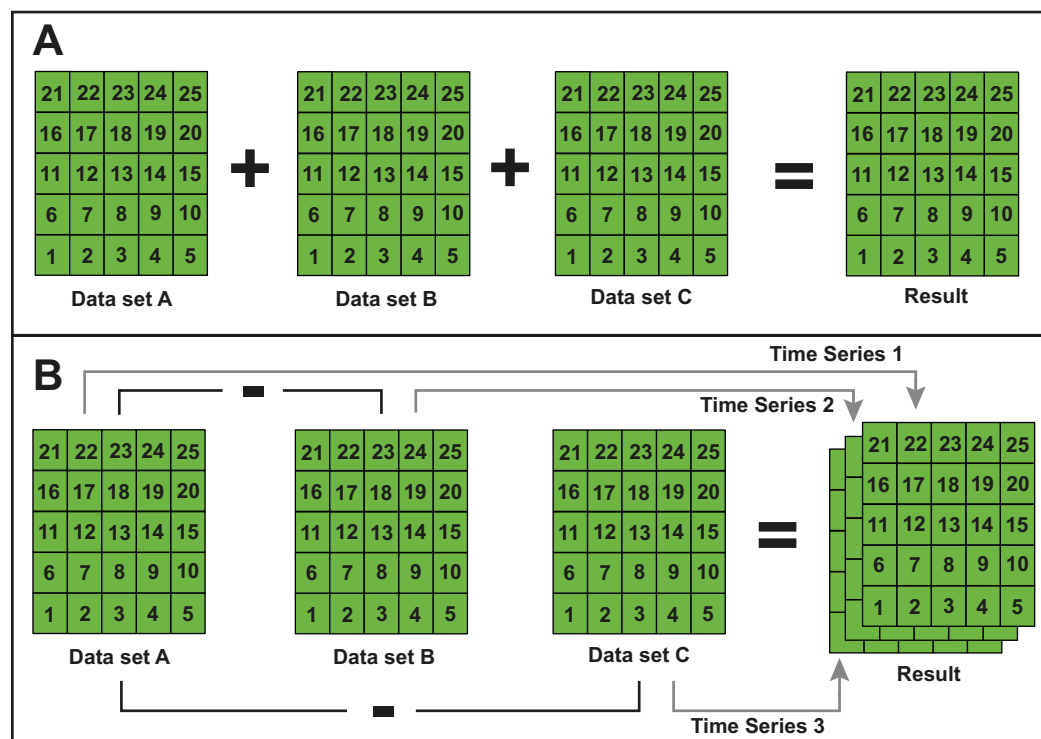


Figure 12. Conceptual workflows for further processing of multiple contour grids. (A) Describes the result of the “topology calculator” tool after using an addition operation on each contour grid (e.g., Data set A + Data set B + Data set C = Result). (B) Describes the “topology time series” tool, which calculates a progression of results to show differences between Data set A, Data set B and Data set C. The result is a progression from Time Series 1 (Data set A) to Time Series 2 (Data set A–Data set B) to Time Series 3 (Data set A–Data set B–Data set C). Note that the “topology calculator” and “topology time series” tools are both based on contour grids that use the same sample area identifiers for each grid square.

- The ability to create contour grid plots that map and visualize spatial variations of numerous network properties such as fracture intensity, connectivity, block distribution statistics, etc.; and
- Topology calculator and time series functionality for comparison between different fracture populations and their statistics.

It is our hope that the NetworkGT toolbox will help facilitate the increasing application of geometry and topology in the analysis and comparison of two-dimensional fracture networks. The integration of the toolbox into an ArcGIS environment allows two-dimensional fracture networks to be interpreted, mapped, and analyzed within the same software package.

ACKNOWLEDGMENTS

We thank test users, Luisa Zuluaga and Tor Storstein, for useful comments on earlier versions of the NetworkGT Toolkit. Nyberg is supported by Statoil ASA through the Sedimentology and Basin Analysis (project no. 810127). Nixon is supported by a VISTA scholarship (project no. 6265) from the Norwegian Academy of Science and Letters. We acknowledge useful comments from colleagues within the ANIGMA project, which is funded from the Research Council of Norway (project no. 244129/E20) through the ENERGIX program and from Statoil ASA through the Ak-

ademia agreement. The anonymous reviewer and editor, Prof. de Silva, are thanked for their constructive comments.

REFERENCES CITED

- Adler, P.M., and Thovert, J.F., 1999, *Fractures and Fracture Networks*: Dordrecht, Kluwer Academic Publishers, <https://doi.org/10.1007/978-94-017-1599-7>.
- Adler, P.M., Thovert, J.F., and Mourzenko, V.V., 2013, *Fractured Porous Media*: Oxford, UK, Oxford University Press, 184 p.
- Alberti, M., 2005, Application of GIS to spatial analysis of mesofault populations: *Computers & Geosciences*, v. 31, p. 1249–1259, <https://doi.org/10.1016/j.cageo.2005.03.013>.
- Bemis, S.P., Micklethwaite, S., Turner, D., James, M.R., Akciz, S., Thiele, S.T., and Bangash, H.A., 2014, Ground-based and UAV-based photogrammetry: A multi-scale, high-resolution mapping tool for structural geology and paleoseismology: *Journal of Structural Geology*, v. 69, p. 163–178, <https://doi.org/10.1016/j.jsg.2014.10.007>.
- Berkowitz, B., 2002, Characterizing flow and transport in fractured geological media: A review: *Advances in Water Resources*, v. 25, no. 8–12, p. 861–884, [https://doi.org/10.1016/S0309-1708\(02\)00042-8](https://doi.org/10.1016/S0309-1708(02)00042-8).
- Bhattacharyya, P., and Czeck, D.M., 2008, Using network analyses within geographic information system technologies to quantify geometries of shear zone networks: *Geosphere*, v. 4, p. 640–656, <https://doi.org/10.1130/GES00124.1>.

- Bisdom, K., Nick, H.M., and Bertotti, G., 2017, An integrated workflow for stress and flow modelling using outcrop-derived discrete fracture networks: *Computers and Geosciences*, v. 103, p. 21–35, <https://doi.org/10.1016/j.cageo.2017.02.019>.
- Bonnet, E., Bour, O., Odling, N.E., Davy, P., Main, I., Cowie, P., and Berkowitz, B., 2001, Scaling of fracture systems in geological media: *Reviews of Geophysics*, v. 39, no. 3, p. 347, <https://doi.org/10.1029/1999RG000074>.
- Dimmen, V., Rotevatn, A., Peacock, D.C.P., Nixon, C.W., and Nærland, K., 2017, Quantifying structural controls on fluid flow: Insights from carbonate-hosted fault damage zones on the Maltese Islands: *Journal of Structural Geology*, v. 101, p. 43–57, <https://doi.org/10.1016/j.jsg.2017.05.012>.
- ESRI, 2016, ArcGIS, version 10.4: Redlands, California, Environmental Systems Research Institute.
- Fadakar-A, Y., 2017, ADFNE: Open Source Software for Discrete Fracture Network Engineering, Two and Three Dimensional Applications: *Computers and Geosciences*, v. 102, p. 1–11, <https://doi.org/10.1016/j.cageo.2017.02.002>.
- Fisher, N.I., 1993, *Statistical Analysis of Circular Data*, Volume 18: New York, Cambridge University Press, 277 p., <https://doi.org/10.1017/CBO9780511564345>.
- FracMan7, 2012, FracMan7, 2012: Golder Associates Inc., <http://www.golder.com>.
- Gillespie, P.A., Howard, C.B., Walsh, J.J., and Watterson, J., 1993, Measurements and characterization of spatial distributions of fractures: *Tectonophysics*, v. 226, p. 113–141, [https://doi.org/10.1016/0040-1951\(93\)90114-Y](https://doi.org/10.1016/0040-1951(93)90114-Y).
- Hardebol, N.J., and Bertotti, G., 2013, DigiFract: A software and data model implementation for flexible acquisition and processing of fracture data from outcrops: *Computers & Geosciences*, v. 54, p. 326–336, <https://doi.org/10.1016/j.cageo.2012.10.021>.
- Harper, M., Weinstein, B., Simon, C., chebee7i, Swanson-Hysell, N., The Gitter Badger, Greco, M., and Zuidof, G., 2015, Python-ternary: Ternary Plots in Python: Zenodo, doi:10.5281/zenodo.34938.
- Healy, D., Rizzo, R.E., Cornwell, D.G., Farrell, N.J.C., Watkins, H., Timms, N.E., Gomez-Rivas, E., and Smith, M., 2016, FracPaQ: A MATLAB toolbox for the quantification of fracture patterns: *Journal of Structural Geology*, v. 95, p. 1–16, <https://doi.org/10.1016/j.jsg.2016.12.003>.
- Huseby, O., Thovert, J.-F., and Adler, P.M., 1997, Geometry and topology of fracture systems: *Journal of Physics. A, Mathematical and General*, v. 30, p. 1415–1444, <https://doi.org/10.1088/0305-4470/30/5/012>.
- Jing, L., and Stephansson, O., 1997, Network topology and homogenization of fractured rocks, in Jamtveit, B., and Yardley, B.W., eds., *Fluid Flow and Transport in Rocks: Mechanisms and Effects*: Oxford, Chapman & Hall, p. 191–202, https://doi.org/10.1007/978-94-009-1533-6_11.
- Johnston, J.D., and McCaffrey, K.J.W., 1996, Fractal geometries of vein systems and the variation of scaling relationships with mechanism: *Journal of Structural Geology*, v. 18, no. 2–3, p. 349–358, [https://doi.org/10.1016/S0191-8141\(96\)80055-1](https://doi.org/10.1016/S0191-8141(96)80055-1).
- Kim, Y.-S., and Sanderson, D.J., 2005, The relationship between displacement and length of faults: A review: *Earth-Science Reviews*, v. 68, p. 317–334, <https://doi.org/10.1016/j.earscirev.2004.06.003>.
- Kociánová, L., and Melichar, R., 2016, OATools: An ArcMap add-in for the orientation analysis of geological structures: *Computers & Geosciences*, v. 87, p. 67–75, <https://doi.org/10.1016/j.cageo.2015.12.005>.
- Manzocchi, T., 2002, The connectivity of two-dimensional networks of spatially correlated fractures: *Water Resources Research*, v. 38, no. 9, <https://doi.org/10.1029/2000WR000180>.
- Mauldon, M., Dunne, W.M., and Rohrbaugh, M.B., 2001, Circular scanlines and circular windows: new tools for characterizing the geometry of fracture traces: *Journal of Structural Geology*, v. 23, p. 247–258, [https://doi.org/10.1016/S0191-8141\(00\)00094-8](https://doi.org/10.1016/S0191-8141(00)00094-8).
- McCaffrey, K.J.W., Jones, R.R., Holdsworth, R.E., Wilson, R.W., Clegg, P., Imber, J., Holliman, N., and Trinks, I., 2005, Unlocking the spatial dimension: digital technologies and the future of geoscience fieldwork: *Journal of the Geological Society of London*, v. 162, p. 927–938, <https://doi.org/10.1144/0016-764905-017>.
- Morley, C.K., and Nixon, C.W., 2016, Topological characteristics of simple and complex normal fault networks: *Journal of Structural Geology*, v. 84, p. 68–84, <https://doi.org/10.1016/j.jsg.2016.01.005>.
- Nixon, C.W., 2013, *Analysis of Fault Networks and Conjugate Systems* [Ph.D. thesis]: Southampton, UK., University of Southampton, p. 75–111.
- Nixon, C.W., Sanderson, D.J., and Bull, J.M., 2011, Deformation within a strike-slip fault network at Westward Ho! Devon U.K.: Domino vs. conjugate faulting: *Journal of Structural Geology*, v. 33, p. 833–843, <https://doi.org/10.1016/j.jsg.2011.03.009>.
- Nixon, C.W., Sanderson, D.J., and Bull, J.M., 2012, Analysis of a strike-slip fault network using high resolution multibeam bathymetry, offshore NW Devon U.K.: *Tectonophysics*, v. 541–543, p. 69–80.
- Nixon, C.W., Bull, J.M., and Sanderson, D.J., 2014, Localized vs. distributed deformation associated with the linkage history of an active normal fault, Whakatane Graben, New Zealand: *Journal of Structural Geology*, v. 69, p. 266–280, <https://doi.org/10.1016/j.jsg.2014.06.005>.
- Nyberg, B., Buckley, S.J., Howell, J.A., and Nanson, R.A., 2015, Geometric attribute and shape characterization of modern depositional elements: A quantitative GIS method for empirical analysis: *Computers & Geosciences*, v. 82, p. 191–204, <https://doi.org/10.1016/j.cageo.2015.06.003>.
- Peacock, D.C.P., Nixon, C.W., Rotevatn, A., Sanderson, D.J., and Zuluaga, L.F., 2016, Glossary of fault and other fracture networks: *Journal of Structural Geology*, v. 92, p. 12–29, <https://doi.org/10.1016/j.jsg.2016.09.008>.
- Pickering, G., Bull, J.M., and Sanderson, D.J., 1995, Sampling power-law distributions: *Tectonophysics*, v. 248, p. 1–20, [https://doi.org/10.1016/0040-1951\(95\)00030-Q](https://doi.org/10.1016/0040-1951(95)00030-Q).
- Priest, S.D., 1993, *Discontinuity Analysis for Rock Engineering*: New York, Chapman and Hall, p. 473, <https://doi.org/10.1007/978-94-011-1498-1>.
- Procter, A., and Sanderson, D.J., 2018, Spatial and layer-controlled variability in fracture networks: *Journal of Structural Geology*, v. 108, p. 52–65, <https://doi.org/10.1016/j.jsg.2017.07.008>.
- Putz-Perrier, M.W., and Sanderson, D.J., 2008, Spatial distribution of brittle strain in layered sequences: *Journal of Structural Geology*, v. 30, p. 50–64, <https://doi.org/10.1016/j.jsg.2007.10.005>.
- Putz-Perrier, M.W., and Sanderson, D.J., 2010, Distribution of faults and extensional strain in fractured carbonates of the North Malta Graben: *American Association of Petroleum Geologists Bulletin*, v. 94, p. 435–456, <https://doi.org/10.1306/08260909063>.
- Richards, F.L., Richardson, N.J., Bond, C.E., and Cowgill, M., 2015, Interpretational variability of structural traps: implications for exploration risk and volume uncertainty, in Richards, F.L., et al., eds., *Industrial Structural Geology: Principles, Techniques, and Integration*: Geological Society of London, Special Publications, v. 421, p. 7–27, <https://doi.org/10.1144/SP421.13>.
- Rohrbaugh, M.B., Dunne, W.M., and Mauldon, M., 2002, Estimating fracture trace intensity, density, and mean length using circular scan lines and windows: *American Association of Petroleum Geologists Bulletin*, v. 86, p. 2089–2104.
- Sanderson, D.J., and Nixon, C.W., 2015, The use of topology in fracture network characterization: *Journal of Structural Geology*, v. 72, p. 55–66, <https://doi.org/10.1016/j.jsg.2015.01.005>.
- Terzaghi, R.D., 1965, Sources of error in joint surveys: *Geotechnique*, v. 15, p. 287–304, <https://doi.org/10.1680/geot.1965.15.3.287>.
- Torabi, A., and Berg, S.S., 2011, Scaling of fault attributes: A review: *Marine and Petroleum Geology*, v. 28, p. 1444–1460, <https://doi.org/10.1016/j.marpetgeo.2011.04.003>.
- Watkins, H., Bond, C.E., Healy, D., and Butler, R.W., 2015, Appraisal of fracture sampling methods and a new workflow to characterise heterogeneous fracture networks at outcrop: *Journal of Structural Geology*, v. 72, p. 67–82, <https://doi.org/10.1016/j.jsg.2015.02.001>.
- Zeeb, C., Gomez-Rivas, E., Bons, P.D., Virgo, S., and Blum, P., 2013, Fracture network evaluation program (FraNEP): A software for analyzing 2D fracture trace-line maps: *Computers & Geosciences*, v. 60, p. 11–22, <https://doi.org/10.1016/j.cageo.2013.04.027>.
- Zimmerman, R., and Main, I., 2003, Hydromechanical behavior of fractured rocks, in Guéguen, Y., and Boutéca, M., ed., *Mechanics of Fluid Saturated Rocks*: Academic Press, International Geophysics Series, v. 89, p. 361–419.